K.-D. Gottschaldt, U. Walzer, R. Hendel, D. R. Stegman, J. R. Baumgardner, and H.-B. Mühlhaus. Stirring in 3-d spherical models of convection in the Earth's mantle. Philosophical Magazine, 86: 3175-3204, 2006.

Stirring in 3-d spherical models of convection in the Earth's mantle

K.-D. Gottschaldt (1), U. Walzer (2), R. F. Hendel (2), D. R. Stegman (3), J. R. Baumgardner (4), H.-B. Mühlhaus (1)

(1) University of Queensland, ESSCC, PO Box 6067, St Lucia QLD 4067, Australia
(2) Friedrich-Schiller-Universität Jena, Institut für Geowissenschaften, Burgweg 11, 07749 Jena, Germany
(3) Monash University, MC^2, Victoria 3800, Australia
(4) University of California, Department of Earth & Planetary Science, 307 McCone Hall, Berkeley, CA 94720-4767, USA

email: k.gottschaldt@uq.edu.au

Abstract

On a global scale basalts from mid-ocean ridges are strikingly more homogeneous than basalts from intraplate volcanism. The observed geochemical heterogeneity argues strongly for the existence of distinct reservoirs in the Earth's mantle. It is an unresolved problem of Geodynamics how these findings can be reconciled with large-scale convection. We review observational constraints, and investigate stirring properties of numerical models of mantle convection.

Conditions in the early Earth may have supported layered convection with rapid stirring in the upper layers. Material that has been altered near the surface is transported downwards by small-scale convection. Thereby a layer of homogeneous depleted material develops above pristine mantle.

As the mantle cools over Earth history, the effects leading to layering become reduced and models show the large-scale convection favoured for the Earth today. Laterally averaged, the upper mantle below the lithosphere is least affected by material that has experienced near-surface differentiation. The geochemical signature obtained during the previous episode of small-scale convection may be preserved there for the longest time. Additionally stirring is less effective in the high viscosity layer of the central lower mantle (Walzer et al., 2003, 2004a), supporting the survival of medium-scale heterogeneities there.

These models are the first, using 3-d spherical geometry and Earth-like parameters, to address the suggested change of convective style. Although the models are still far from reproducing our planet, we find that proposal might be helpful towards reconciling geochemical and geophysical constraints.

1. Introduction

The existence of geochemically distinct reservoirs in the Earth's mantle is inferred from the observation of worldwide rather homogeneous mid-ocean ridge basalts (MORB) on the one hand and heterogeneous ocean island basalts (OIB) on the other (Zindler and Hart, 1986, Silver et al., 1988, Hart and Zindler, 1989, Allègre and Lewin, 1995, Hofmann, 1997). Of course, what we observe today is the result of the interplay between chemical differentiation and convective stirring that started with the formation of the Earth and is still going on.

Seismic tomography provides a snapshot of the modern mantle. Wave speed anomalies are interpreted as evidence for subducting slabs that extend from the surface to the lower or lowermost mantle (Grand et al., 1997, van der Hilst and Kárason, 1999, Masters et al., 2000, Trampert et al, 2004) and for superplume upwellings from the core mantle boundary (CMB) region (Su et al, 1994, Ritsema et al., 1999, 2000). Together with the prevailing surface plate

velocities these seismic observations lead most investigators to conclude there has been considerable mass exchange between upper and lower layers of the mantle for at least the last 100 Ma.
The reconciliation of geochemical and geophysical evidence has long been an unresolved problem in geodynamics. How can different geochemical reservoirs be maintained in the presence of large-scale convection for a long time? Why is one part of the mantle more homogeneous on a global scale than other parts?
This paper is a contribution towards a self-consistent thermochemical evolution model of the Earth. A crude approximation for crustal differentiation is coupled to numerical models of global mantle convection, focussing on geometrical effects and the influence of rheology on stirring.
In the following section we review geochemical and geophysical constraints as well as proposals for their reconciliation. The methodology adopted for numerical modelling of thermal convection and treatment of compositional fields is described thereafter. In the main part of the paper we introduce results of selected models and discuss them. We highlight results that could be relevant for the Earth in the final section and point out some possible future research directions.

2. Structure of the Earth's mantle

Any successful model must satisfy the observational constraints. The following compilation of knowns and unknowns may help to weigh the relevance of the various alternative models.

2.1. Geophysical and geological constraints

2.1.1. Plate tectonics

The relevance to the Earth of a convective stirring model depends strongly on the realism of the assumed solid-state creep velocity field. In addition to hints from tomographic images we can directly observe the surface planform of the current surface velocity field that consists of about 25 rigid tectonic plates separated by narrow linear high strain zones where plates move relative to one another (e.g. Kreemer et al., 2002). The degree of dynamic coupling between the plates and other parts of the mantle, however, is not yet entirely clear. From reconstruction of past plate movements and given the fact of decreasing internal heating, it follows that mantle convection is time-dependent. But this surface motion history is known reliably for no more than 120 Ma. The tectonic style of the early Earth is largely unknown. Proposed alternatives to plate tectonics for the early Earth include episodic resurfacing (van Thienen, 2003) and the plughole model (Trendall, 2002).

2.1.2. Formation of crust

Its peculiar twin-peaked hypsometric curve sets Earth apart from other terrestrial planets. There is thin (0 - 7 km) oceanic crust (OC) that is continuously generated at mid-ocean ridges and recycled almost entirely back into the mantle at subduction zones. By contrast, continental crust (CC) is less dense and thicker (~40 km). It is buoyant and recycled into the mantle only to a small degree, as sediments or by delamination. While the lifetime of OC is about 100 Ma, that of CC is at least 2 Ga (Hofmann, 1997). Suggestions for the segregation history of CC range from rapid early net growth to episodic growth of juvenile CC to continuous net growth (review by Arndt, 2004). Today CC is produced mainly by andesitic volcanism related to subduction and the release of water from the slab. Continents themselves also grow through intraplate volcanism and the accretion of sediments and basaltic terranes. Such terranes could be the product of extensive melting caused by plume heads reaching the surface (Hofmann, 1997). Tectonic settings for the formation of Archean cratons may have been different and include rifts (Trendall, 2002, van

Thienen, 2003), but are still represent on the extraction of partial melt from the shallow (< 200 km: Presnall et al., 2002) mantle.

2.1.3. Seismology

Small-scale upwellings from the deeper mantle are thought to cause OIB volcanism. Tomographic imaging of these plumes suggests different sampling depths, from the CMB to the transition zone (Courtillot et al., 2003, Montelli et al., 2004).
Besides the phase transitions at 410 and 660 km depth there is a seismic discontinuity 200 - 300 km above the CMB. This so-called D" layer has pronounced topography and could represent dense, recycled OC (Christensen and Hofmann, 1994), sunken primordial crust (Tolstikhin and Hofmann, 2004), a phase transition (Sidorin et al., 1999, Oganov and Ono, 2004) or a combination of these.
There is evidence that compositional effects contribute to the heterogeneity of tomographic images, especially in the lower third of the mantle (Trampert et al., 2004).

2.1.4. Convective mixing

Heterogeneities in a convecting fluid are deformed by stirring and finally erased by diffusive mixing. Chemical diffusion in mantle rock acts on the scale of centimetres over the lifetime of the Earth, but our models resolve km-scales. Thefore this paper deals only with convective stirring. Some nice studies about mantle stirring and mixing in 2-d have been done (e.g. Christensen, 1989, Gurnis and Davies, 1986, Kellogg and Stewart, 1991; Kellogg and Turcotte, 1990, Metcalfe et al., 1995, Olson et al., 1984, Ottino, 1989, Ten et al., 1996, 1997, 1998). Unfortunately, results from studies in 2-d can be extrapolated to 3-d only in a limited manner. Tracers in 3-d poloidal stationary convection move on 2-d toruslike surfaces. Stirring is constrained to these surfaces. Cross-cell stirring becomes possible in time-dependent flows, but is not very efficient (Schmalzl, 1996). Large-scale stirring is enhanced by a toroidal component, but convectively isolated islands of laminar stirring may remain (Ferrachat and Ricard, 1998). Convection in the Earth is time-dependent and the surface planform shows a strong toroidal component today (O'Connell et al., 1991). Since there is currently no general understanding about the stirring behaviour of the mantle, a case-by-case study of different models is necessary.

2.2. Geochemical constraints

2.2.1. Geochemical heterogeneities

Observed geochemical heterogeneities range from cm-scale structures in high-temperature peridotites (Allègre and Turcotte, 1986) to the DUPAL anomaly (Hart, 1984). The latter seems to have a different origin in the Pacific than in the southern Atlantic and Indian Ocean (Hanan et al., 2004), so it is not global. Yet its existence for at least 115 Ma (Weiss et al., 1989) indicates that there is limited large-scale lateral stirring somewhere in the mantle.
The OIB isotopic compositions are far more diverse than MORB compositions (e.g. Allègre, 2002), with the global variance of isotopic ratios for OIB being three times larger than the corresponding global variance of MORB (Allègre et al., 1987). The degree to which mantle heterogeneities are reflected in the resulting basalt depends on the degree of partial melting, magma mixing and extraction, the size of the volume that is sampled by partial melt, and the dimension of geochemical heterogeneity itself. Differences in composition and heterogeneity between OIB and MORB could be due to different sampling processes (Meibom and Anderson, 2003), sampling of different geochemical reservoirs (e.g. Hofmann, 1997) or a combination of these (Kellogg et al., 2002). The concept of a reservoir is here used to reflect a scale of systematic variation of mantle geochemistry that is too large to be erased by the sampling process. Sampling

at mid-ocean ridges, for instance, acts on a scale of 30 – 200 km in depth and several hundred kilometres in width (e.g. Presnall et al., 2002) and hence the scale of the implied reservoir is larger.

2.2.2. Mantle degassing

From the amount of ^{40}Ar in the atmosphere it has been estimated, that only about 50 % of this isotope have been degassed from the mantle (Allègre et al., 1996). The low concentration in MORB suggests there is another reservoir containing the missing ^{40}Ar. This is a strong argument against simple whole-mantle convection (Hofmann, 1997). However, it is subject to challenge, because the amount of ^{40}K in the Earth (Coltice and Ricard, 2002) and the role of Ar-recycling (Rüpke et al., 2003) are poorly constrained.
That nearly all the ^{3}He coming from the mantle is likely primordial also supports the conclusion that the Earth has never been completely degassed. The ratio ^{3}He/^{4}He is very uniform in MORB, but varies in OIB. There must be a source of absolutely high ^{3}He concentration, possibly 3.5 times higher than currently estimated from He flux (Ballentine et al., 2002). Besides poorly degassed or primordial mantle, the core could also be a source for ^{3}He (Walzer et al., 2004b). High ^{3}He/^{4}He signatures may form in recycled material too, if it is convectively isolated long enough (Ferrachat and Ricard, 2001).

2.2.3. Interpretation of reservoirs

The MORB source region is sampled by the network of divergent margins all over the world and therefore is thought to occupy the shallow mantle (Hofmann, 1997). The fixity of OIB-producing hot spots relative to surface plate movements is a compelling indicator that these plumes originate in and sample deeper regions of the mantle that are more or less decoupled from the surface motion. This is independently supported by tomographic images of deep-rooted plumes under OIB hot spots (Montelli et al., 2004), but hard to reconcile with a proposed (Meibom and Anderson, 2003) shallow origin for all geochemical heterogeneity.
The roughly complementary geochemical signatures of CC and MORB are interpreted to be the result of primary extraction of CC from the original primitive mantle (PM). Mixing of all OIB would not give MORB. Other reservoirs proposed to contribute to OIB in differing proportions are EM1, EM2 (enriched mantle) and HIMU (high $\mu = {}^{238}\mathrm{U}/{}^{204}\mathrm{Pb}$). HIMU could be subducted oceanic crust, EM1 delaminated lower CC (Hofmann, 1997) or subducted oceanic plateaus (Albarède, 2001) and EM2 subducted continental sediments. The MORB source (depleted MORB mantle, DMM) is variably polluted on a regional scale by other components (Hanan et al., 2004). However, the absence of PM samples does not preclude the existence of a primitive reservoir (Kellogg et al., 2002).

2.2.4. Age of reservoirs

The mean age of CC is 2 - 2.5 Ga, and that of oceanic basalts 1 – 1.3 Ga (Hofmann, 1997), but latter is not necessarily the age of original differentiation (Albarède, 2001). The oldest HIMU signature is about 2 Ga (Hofmann, 1997). Not introducing HIMU into the mantle prior to 2 - 2.5 Ga before present, due to a change in the surface oxidization environment or to subduction zone processes, could explain that age (Xie & Tackley, 2003). The coincidence with the assumed end of primary CC segregation is striking.

2.2.5. Size of reservoirs

How much of the mantle must have been depleted in incompatible elements to form the present volume of CC? Estimates depend on the geochemical models used for CC, depleted mantle (DM, with or without OIB), and bulk silicate Earth (BSE) and range from 25 – 90 % (Hofmann, 1997), but more likely 40 - 50 % (Allègre, 2002). There must be one or more reservoir(s) containing the missing elements, in particular, the heat-producing nuclides (^{235}U, ^{238}U, ^{40}K, ^{232}Th) and ^{40}Ar (Albarède and van der Hilst, 2002). Additionally, the amount of heat-producing nuclides in MORB is too small to explain the present heat flux from the mantle and there is less ^{4}He degassing than would be expected from the decay of heat-producing nuclides as well (O'Nions and Oxburgh, 1983, van Keken et al., 2001). The hidden reservoir could be primordial. The heat-helium imbalance and missing ^{40}Ar-paradox would disappear if the concentration of ^{3}He in the mantle were higher than previous estimates (Ballentine et al., 2002).

2.3. Reconciliation of geophysical and geochemical constraints

There are several proposals how the depleted, well-mixed DMM could be separated from the other reservoirs and evolve independently for billions of years.

2.3.1. Phase boundaries

The γ-spinel-to-perovskite-plus-magnesiowüstite phase transition at 660 km depth hinders convection. It is appealing from a geochemical point of view to assume that it forces the upper mantle to convect separately from the lower mantle, but results of seismic tomography (e.g. van der Hilst et al., 1997, Masters et al., 2000, Trampert et al., 2004) show penetration of the boundary today. On the other hand, temporal layering has been proposed on geological (e.g. Condie, 1997) geophysical (Breuer and Spohn, 1995) and geochemical (Hofmann, 1997, Allègre, 1997, 2002) grounds. The necessary change in the effect of the phase transition could be due to the temperature-dependence of the Clapeyron slope (Hirose, 2002) or the decreasing Rayleigh number (Ra) of the Earth (e.g. Tackley, 1996). However, at the Ra range assumed for the Earth, dynamic models commonly show avalanches through the phase boundary rather than long-term layering (Tackley, 1996).

2.3.2. Small-scale heterogeneities plus D"

The assumption that large-scale convection implies very efficient stirring leads to a cartoon with nearly the entire mantle being homogeneous DMM. Only D" remains as a possible repository of enriched reservoirs and hence as the OIB source region (e.g. Stegman et al., 2002). OIB plumes originating at shallower depths (Montelli et al., 2004) are an argument against this model. Additionally, D" is a rather small volume in which to fit all the heterogeneities (Hofmann, 1997, Albarède and van der Hilst, 2002). On the other hand, by assuming that the 'homogeneous' mantle is riddled with small scale (~ 8 km: Helffrich and Wood, 2001) up to regional scale (~ 100 km: Meibom and Anderson, 2003) blobs of recycled material, the model becomes geochemically somewhat more plausible. Coltice and Ricard (2002) suggest a marble-cake mantle with recycled OC and peridotites containing primitive veins. In this case the mantle is assumed merely to be better mixed within the MORB source region than below it. Differing geochemical signatures are formed by mixing different amounts of these components, and because of segregation of dense OC, possibly in D". Heterogeneities smaller or comparable to the scale of sampling are supported by observations, but larger scale heterogeneities also exist (Trampert et al., 2004). None of above models, however, conclusively explains the coexistence of a shallow, more homogeneous reservoir and a deeper, less mixed one.

2.3.3. Different intrinsic densities

Because of its heterogeneity and topography, higher internal density of the D" layer is a likely explanation for its stability at the bottom of the convecting mantle. Compared to buoyancy, effects of a post-perovskite phase transition are probably small (Nakagawa and Tackley, 2004). If D" is made of subducted OC (eclogite), it could be the HIMU reservoir (Hofmann, 1997). If it is foundered early crust (Tolstikhin and Hofmann, 2004), D" could serve as a source for primordial gases and missing incompatible elements.
A stable dense layer at 1500 - 2000 km depth was put forward by Kellogg et al. (1999) and could represent a leftover feature from the mantle's early evolution, e.g., magma ocean crystallisation (Hofmann, 1997). Its seismic invisibility combined with fluid-dynamical constraints, however, weighs against the presence of such a layer today (e.g. Oldham, 2004).
Dense material near the CMB could also be swept into 'piles' beneath upwellings and thinned, possibly to zero, under downwellings (Tackley, 2000). This model is consistent with seismic tomography (Tackley, 2002, Trampert et al., 2004), but the volume of the piles is still rather small to satisfy geochemical constraints (Hofmann, 1997). It is not known whether dense piles can be formed and maintained by modern tectonic processes at the surface, or by core-mantle interactions, or represent a leftover expression of magma ocean fractional crystallisation, or a combination of these (van der Hilst, 2004). Geodetic results contradict the expected CMB depression under dense piles (Forte et al, 1995). However, CMB topography is currently poorly constrained (Schweitzer, 2002).
Chemical zoning in the mantle can develop if subducted oceanic plates loaded with OIB would sink deeper than pure OC (Albarède and van der Hilst, 2002). The selectivity of this mechanism is reduced, however, by the dependence on the thermal state and tectonic setting of the plate, which is not directly correlated to its load of plume heads. It remains to be determined whether the latter model is adequate to explain the coexistence and age of homogeneous MORB- and heterogeneous OIB-sources.

2.3.4. Viscosity contrasts

Blobs having a 10 – 100 times higher viscosity resist stretching and mixing by the surrounding mantle (Manga, 1996). It is conceivable, that 35 – 65 % of the mantle could consist of such PM blobs and be concentrated in the LM (Becker et al., 1999). The lack of sampling of any such PM components at mid ocean ridges and their need for persisting negative or neutral buoyancy despite substantial heating internal to the blobs are arguments against the model.
Other studies focus on radial viscosity stratification. Neither sufficient layering in the stirring efficiency (Stegman et al., 2002) nor significant convective isolation (van Keken and Ballentine, 1998, van Keken and Zhong, 1999, Ferrachat & Ricard, 2001) were found for moderate viscosity contrasts. A model with more extreme contrasts (> factor of 1000) developed small-scale dominated whole mantle convection and separate reservoirs for DMM and PM, but no deep subduction (Walzer and Hendel, 1999).
Allègre (2002) surmises that vigorous convection in the asthenosphere and sluggish stirring in the high viscosity transition layer both contribute to maintaining the MORB source region

2.3.5. Filtering in the transition zone

The solubility of water above the β-to-γ-spinel transition is smaller than in the transition zone beneath it. Water lost from rising material lowers the melting temperature, possibly leading to a thin layer of partial melt at 410 km depth. Melt at that depth is denser than the matrix and will not rise. Incompatible elements concentrate in the melt and therefore only depleted material would reach the shallow mantle (Bercovici and Karato, 2003). This hypothised filtering mechanism must be less efficient in hotter environments, allowing OIB forming plumes to retain enriched

signatures. The temperature dependence would also allow CC to be formed from a volume larger than that above the transition zone.

3. Methodology

3.1. Numerical modelling of thermal convection

The thermal convection part of the models described in this paper is based on Walzer et al. (2003b, 2004a). A more extensive description is given there. Symbols and parameters are explained in the text where they first occur. Radial reference profiles are denoted by index *r*.

3.1.1. Basic equations

Thermal convection is based on the conservation laws for energy, momentum and mass, plus an equation of state. The energy equation is used in the following formulation:

$$\frac{\partial T}{\partial t} = -\frac{\partial\left(T v_j\right)}{\partial x_j} - \left(\gamma - 1\right)\cdot T\frac{\partial v_j}{\partial x_j} + \frac{1}{\rho c_v}\left[\tau_{ik}\frac{\partial v_i}{\partial x_k} + \frac{\partial}{\partial x_j}\left(k\frac{\partial}{\partial x_j}T\right) + \rho H\right] \tag{1}$$

with T being temperature, v solid state creeping velocity, x a Cartesian coordinate, γ the Grüneisen parameter, k = 12 W m^{-1} K^{-1} the thermal conductivity, c_V the specific heat at constant volume and H the heat generation rate per unit volume. Viscosity η depends on longitude φ, latitude θ, radius r and time t and is included in the deviatoric stress tensor

$$\tau_{ik} = \eta\left(\frac{\partial v_i}{\partial x_k} + \frac{\partial v_k}{\partial x_i} - \frac{2}{3}\frac{\partial v_j}{\partial x_j}\delta_{ik}\right). \tag{2}$$

δ_{ik} is the Kronecker unit tensor. The density ρ is calculated as a variation of a reference profile $\rho_r(r)$, which is taken from PREM (Dziewonski and Anderson, 1981) and therefore contains jumps at the depths of phase transitions:

$$\rho = \rho_r\left[1 - \alpha\left(T - T_r\right) + \frac{p - p_r}{K_T}\right] \tag{3}$$

p denotes the pressure, K_T the bulk modulus and α the coefficient of thermal expansion. Dynamic effects caused by deformation of the phase boundaries in 410 and 660 km depth (Schubert et al., 2001, Turcotte and Schubert, 2002) can not be resolved on our computing grid, but the additional buoyancy is estimated at the respective grid points by

$$F_B = \Gamma\cdot\frac{\Delta\rho}{\rho}\cdot A\cdot\left(T_{av} - T\right) \tag{4}$$

A is the planform area of a grid cell and T_{av} the average temperature of a radial layer. We use the following parameters: Clapeyron slope of the olivine-spinel phase transition Γ_{440} = 3 MPa K^{-1}, associated density jump $\Delta\rho/\rho_{440}$ = 0.0547, Clapeyron slope of the spinel-perovskite transition Γ_{660} = -4 MPa K^{-1}, density jump $\Delta\rho/\rho_{660}$ = 0.0848. The latent heat from the volume V locally processed through the phase boundary at each time step

$$E_{latent} = T\cdot\frac{\Delta\rho}{\rho}\cdot\Gamma\cdot V \tag{5}$$

is added to the energy balance (1) and influences buoyancy by changing T in (4). An infinite Prandtl number is assumed for the conservation of momentum

$$0 = -\frac{\partial}{\partial x_i}\left(p - p_r\right) + \left(\rho - \rho_r\right)g_i + \frac{\partial}{\partial x_k}\tau_{ik} \tag{6}$$

with gravity $\vec{g}$ only depending on radius. In the equation describing conservation of mass the time-dependence can be neglected due to low creeping velocities in the mantle (anelastic liquid approximation):

$$0 = \frac{\partial}{\partial x_j} \rho v_j \tag{7}$$

The six scalar equations (1), (3), (6) and (7) are used to determine *T, p,* ρ and the three components of $\vec{v}$ in a compressible medium for Earth-like parameters. Heating mode, boundary conditions, initial conditions, rheology, radial profiles and general parameters are discussed in section 4. Our convection calculations are restricted to uniform chemical composition.

3.1.2. Numerics

The coupled system of equations is solved numerically with the well-established Fortran code TERRA (Baumgardner, 1983, Yang, 1997) for the whole evolution of the entire mantle. The computational grid is based on a projection of the regular icosahedron onto a sphere and successive dyadic refinements (Baumgardner and Frederickson, 1985). Concentric copies of such spherical layers of nodes build the domain in radial direction. All models have been run on a grid with 1394250 grid points, corresponding to a spatial resolution on the order of 100 km. Equations (6) and (7) are discretised by finite elements with linear basis functions and solved simultaneously (modified after Ramage and Walthan, 1992) using a multigrid method. The energy equation is discretised by the MPDAT algorithm (Smolarkiewicz, 1984) and integrated with a Runge-Kutta scheme using explicit time stepping. Domain decomposition is used for the parallelisation (Bunge & Baumgardner, 1995) with MPI. TERRA was benchmarked for constant viscosity convection by Bunge et al. (1997) with numerical results of Glatzmaier (1988) for Nusselt numbers, peak temperatures, and peak velocities. A good agreement ($\leq$ 1.5 %) was found. However, strong viscosity variations challenge the stability of the code and results should be interpreted as approximations. No detailed error analysis (e.g. DeVolder et al., 2002) was done.

3.2. Treatment of compositional fields

3.2.1. Passive tracers

There are several methods to approximate the advection of non-diffusive scalar fields in thermal convection (van Keken et al. 1997). We use passive Lagrangian tracers that have no feedback on convection. Since the focus of this study is on large scale stirring, it was sufficient to initialise only two tracers per grid point. More tracers would be necessary for modelling chemical differentiation with active tracers, reproducing local geological features or characterise mixing across different scales (e.g. Ten et al., 1997). For testing case H was repeated, starting with eight tracers per grid point. Without fine tuning nearly every second tracer was lost during the run, still giving twice the standard resolution at the last time step. A spherical harmonic analysis of the chemical field reveals not much structure above degree 30, so we cut it off there. The relevant results (figures 4 & 5) are basically identical to the low resolution run.

Each tracer represents half of the mass of its initial cell and keeps this attribute throughout the entire run. Trajectories of the tracers are calculated synchronous to the integration of the heat equation. They move independently of the TERRA grid, but are continuously re-indexed with respect to the nearest grid point. This allows efficient interpolation between the Lagrangian particles and the local neighbourhood of Eulerian grid points. Memory requirements limit the number of tracers that can be hosted by a single grid point. If a grid point becomes overcrowded, surplus tracers are deleted randomly. With ~ 2 % lost tracers and ~ 5 % empty cells after a typical

evolution run coverage is reasonably good. The accuracy of tracer trajectories was tested with prescribed velocity fields. Deviations from the analytic solution were less than 0.006 %, which means ~10 km for a typical run.

3.2.2. Definition of two components

Here we want to track the dispersion of the material that comes close to the surface ('degasses') and characterise its subsequent distribution in the mantle at discrete time steps. In this framework we shall define two components, degassed tracers and residuum, and apply two constraints in our definition:

1. Each component will comprise 50 % of the mantle at the end of the convection calculation. This ensures the comparability of different models. The half-half distribution is the most sensitive for measuring the state of stirring between two components. Moreover, it has been estimated that about 50% of the mantle must have been processed to extract the present volume of CC (see 2.2.5).
2. It must represent a reasonable approximation for chemical differentiation near the surface. This corresponds to the fact that major differentiation processes like the extraction of CC and degassing are related to partial melting near the Earth's surface. Hence the term 'degassing' is used here for a range of chemical modifications near the surface.

The following algorithm is used to satisfy both constraints: No compositional information is assigned to tracers during the convection calculation, but each tracer remembers its closest approach to the surface. This information is output together with the Cartesian coordinates and the mass of each tracer. In postprocessing, the tracers are ordered according to that distance, starting with the smallest. Then their masses are added successively until the sum has reached 50 % of the mantle mass. The distance attribute of the last tracer incrementing this sum is taken as degassing depth (d_d). In other words, the degassing depth is an output, not an input. All tracers which have been closer to the surface than the degassing depth are assigned the concentration c = 0, while the residuum retains a concentration c = 1. This is identical to ongoing differentiation throughout the run with complete degassing above and none below the degassing depth. The algorithm describes modification of pristine mantle near the surface and degassing of primordial, non-radiogenic gases. It is not necessary to prescribe degassing locations such as mid ocean ridges or volcanoes, because mantle rock can reach the surface only at these locations.

In the next step the tracers are mapped onto a Cartesian grid, which eases further processing. The concentration of undegassed material in each cubic cell is the mean of the concentrations of all the tracers it contains, weighted by their masses.

The corresponding strategy for characterising multicomponent fields, e.g., the multitude of mantle reservoirs, would be to consider the distribution of each component separately and treat all others as residuum.

4. Models

4.1. Parameter space

This study reports results from an ongoing effort to develop refined convection-differentiation models of the Earth. We vary subsystems in complex Earth-like models, assess the influence of each variation in the context of the whole system and retain what we deem to be successful variations in the subsequent model. We adopted this evolutionary-optimisation-like strategy because our models are too expensive for a comprehensive search of parameter space. We recognise that results from simple models may not be valid in future more complex ones. Nevertheless, we view our approach as a rational means for an initial parameter space exploration.

4.1.1. General parameters and reference profiles

Some of our model parameters have been provided already with the equations, Walzer et al. (2003b, 2004a) discuss some of the less obvious choices for parameter values. Radial profiles for p_r, ρ_r, g, K_T were taken from PREM, for c_V (figure 1a) and γ (figure 1b) were derived by Walzer et al. (2003b, 2004a) based on PREM. α is shown in figure 1c, T_r in figure 3a . Lateral variations of ρ are allowed according to (3).

[insert figure 1 about here]

We use three different profiles for the melting temperature T_m (T_m1, T_m2, T_m3) (figure 1d). In T_m1 (Walzer et al., 2003b) the melting temperature is linearly interpolated between 660 km depth and CMB, according to experimental results of Zerr and Böhler (1993, 1994). In T_m2 the melting temperature at the CMB was adjusted to results of Böhler (2000). T_m3 is taken from Walzer et al. (2004a).
The heat generation rate per unit volume due to the decay of ^{40}K, ^{242}Th, ^{235}U, ^{238}U is spatially homogeneous, but decays exponentially with time. Parameters are given in Walzer et al. (2004a).
The observed scale of plumes (Montelli et al., 2004) is on the order of our grid resolution and their existence depends on the strong lateral temperature dependence of viscosity. Therefore, a self-consistent formation of small-scale plumes is not possible in our models. On the other hand, major partial melting is expected only near the surface, possibly above the CMB and near 410 km depth. In order to prevent unrealistically high temperatures, we considered cooling due to volcanism and small-scale plumes in the energy equation of some models. It is active only where $T > T_m$ and can be restricted to certain depths and basically means cutting $T > T_m$ to $T = T_m$ each timestep:

$$\rho \cdot H_{cool} = \rho \cdot c_v \cdot \frac{d\left(T - T_m\right)}{dt} \tag{8}$$

In the module *vol1* cooling is active only in the upper mantle, in *vol2* throughout the entire mantle except the CMB region.

4.1.2. Rheology

Diffusion creep dominates in the lower UM and the LM, so Newtonian rheology is a good approximation there (Karato and Li, 1992; Karato and Wu, 1993; Li et al., 1996). An Arrhenius law describes the temperature dependence of viscosity

$$\eta = \eta_0 \exp\left[\xi \frac{T_m}{T}\right] \tag{9}$$

with $\xi = 17$ (Karato et al., 2001) and $\eta_0 = 10^{21}$ Pa s. The radial variation of $\eta(T)$ has been included in a profile $\eta_r(r)$, which also accounts for pressure dependence and compositional effects in the real Earth. For numerical reasons the lateral variability had to be damped by a factor c_t, which does depend on radius (figure 2a) in some models and is constant in others.

$$\eta(r,\theta,\varphi,t) = \eta_r(r) \cdot \exp\left[c_t(r) \cdot T_m(r) \cdot \left(\frac{1}{T(r,\theta,\varphi,t)} - \frac{1}{T_{av}(r,t)}\right)\right] \tag{10}$$

An effective viscosity η_{eff} like in Richards et al. (2001) was applied to the uppermost 285 km of the mantle in some models, with s being square root of the second invariant of the strain rate tensor and the viscoplastic yield stress σ_y.

$$\eta_{eff} = \min\left[\eta(p,T), \frac{\sigma_y}{2s}\right] \tag{11}$$

This weakening is not affected by c_t, but limited to $\eta_{eff} \geq 0.002 \cdot \eta$. Together with a stiff lithosphere and a soft asthenosphere, this yields a crude approximation for plate tectonic behaviour. It should be noted that η_{eff} is to be determined for $t + \delta t$, so the strain rate invariant s in (11) has to be evaluated at time $t + \delta t$. Since the strain rate at $t + \delta t$ is not known the problem has to be solved iteratively (e.g. Moresi and Solomatov, 1998, Tackley, 1998, Trompert and Hansen, 1998) according to $\min(\eta, \sigma_y / 2s_m^{t+\delta t})$, where $m = 0,1,2,...$ is an iteration counter and $s_0^{t+\delta t} = s^t$. An alternative, incremental formulation, which is second order accurate in s, is obtained by replacing $s^{t+\delta t}$ by $s^{t+\delta t} = s^t + \delta s = s^t + 2\varepsilon_{kl}^t(\varepsilon_{kl}^{t+\delta t} - \varepsilon_{kl}^t)/s^t$. ε_{kl} is the stretching tensor. The approach does not require iterations in each time step. Iterations may be performed occasionally to reduce the residuals.

[insert figure 2 about here]

Different radial profiles $\eta_r(r) = \eta\#$ (figures 2b, c, d) are used. The simplest case, *η1*, is constant 10^{23} Pa s throughout the mantle. *η6* and T_m3 are favoured for the modern mantle and were derived (Walzer et al., 2004b) from PREM by using solid-state physics considerations, thermodynamic relations, the Grüneisen parameter and Lindemann's law. The profile is anchored at 10^{21} Pas in the asthenosphere. That value is higher than assumed for the Earth (Dixon et al., 2004), but reflects our present numerical capabilities. *η2* is an earlier version (Walzer et al., 2003b) of *η6*, with a weaker lithosphere and smoother gradients. Physically more desirable steep gradients were taken out there for numerical reasons. A non-conventional feature of *η2* is a second asthenosphere below the transition zone. This weak layer is omitted in *η3* in order to test its influence on the convection. When applied to models using *η2*, the module based on (11) had virtually no effect. Therefore *η4* and *η5* were introduced, featuring stiffer lithospheres but still keeping gradients smooth. Both are generally weaker than *η6* and can therefore be interpreted to show effects of a supposedly hotter, early mantle. However, no attempt has been made here to address shape and amplitude of the viscosity profile for the Archean mantle. We stress that profiles based on PREM are valid for the modern mantle only and that our present models do not include time dependence in the assumed radial viscosity profile.

4.1.3. Boundary conditions

The computing domain is a thick spherical shell, mimicking the silicate part of the Earth. The inner boundary at r_{CMB} = 3480 km and the outer boundary at r_E = 6371 km are free of tangential stresses, because the viscosities of liquid outer core and atmosphere/hydrosphere are negligible compared to mantle rocks.

A constant temperature of 288 K is assumed for the outer boundary, because it is the mean surface temperature today and there has been liquid water on the surface for at least 3.8 Ga.

Different thermal boundary conditions at the CMB reflect the continuous development of our models rather than being a focus of this paper. Condition *CMB1* means a heat flux of 28.9 mW m^{-2} (Anderson, 1998), temporally (e.g. Schubert et al., 2001) and laterally (Walzer et al., 2003b) constant. This was changed to spatially constant temperature, which is adjusted every time step to ensure a mean heat flux constant in time (*CMB2*). The physically most appealing approach is to couple a parameterised model of the evolution of the core to mantle convection. The heat flux

across the CMB is equalled by secular cooling of inner (IC) and outer core (OC), latent heat from freezing or melting of the IC, release of gravitational potential energy due to the preferred segregation of heavy elements at the IC boundary and the radiogenic heat production of the core. This energy balance was calculated every time step to obtain heat flux and spatially constant temperature at the CMB as well as the radius of the inner core. The core model is based on Labrosse et al. (2001), Labrosse (2003) and described elsewhere (Gottschaldt, 2003). This kind of boundary condition is characterised in the following by the concentration of ^{40}K, which is thought to be the major radiogenic heat source in the core.

4.1.4. Initial conditions

Because of the assumption of infinite Prandtl number and homogeneous composition, we need consider only the initial temperature field. The thermal state of the early Earth is highly speculative, and we have explored several different scenarios. Frequent impacts may have determined the heat structure of the outer layers (Arrhenius and Lepland, 2000), leading to an early thermally stable stratification. A global magma ocean (Solomatov, 2000) or several large scale melting events (Kleine et al., 2004) are also conceivable. Fractional crystallisation and subsequent overturn has the potential to result in compositionally or thermally stable layering, too (Elkins-Tanton et al., 2003, Zaranek and Parmentier, 2004, Ferrachat, personal communication 2004). In this context we used a starting profile of constant temperature $T_{av}(r)$, which is stable in a compressible mantle. Only in the upper boundary layer did we introduce a smooth transition to the surface temperature (figure 3b). Together with a small lateral perturbation of the form

$$T(r,\theta,\varphi) = T_{av}(r) + T(\theta,\varphi)\cdot\cos\left[\frac{\pi}{r_E - r_{CMB}}\cdot\left(r - \frac{r_E + r_{CMB}}{2}\right)\right] \tag{12}$$

with

$$T(\theta,\varphi) = \sum_{l=2}^{15}\sum_{m=1}^{l} 0{,}002\cdot(-1)^m \cdot P_l^m(\cos\theta)\cdot\left[\cos(m\varphi) - \sin(m\varphi)\right] \tag{13}$$

this initial condition is called *IC1*. P_l^m is a Legendre function. The above perturbation is used for all models of this study. In *IC2* a lower thermal boundary layer was added (figure 3c). An adiabatic profile plus boundary layers (Stacey, 1992) and the solidus T_m3 are more obvious starting profiles, used in *IC3* (figure 3d) and *IC4* respectively.

[insert figure 3 about here]

4.2. Results

The ultimate goal of convection-differentiation models is to reproduce observations. For geochemistry this would be plots of isotopic concentrations in surface samples. Since no isotopic systems are modelled, this is not possible here. We focus on large-scale geometrical characteristics of the convective flow instead. For easy comparison, results are grouped together here and will be discussed in the next section. The parameter space covered by this study and some output values are summarized in table 1. Maximum and root mean square (rms) surface velocity may be used to compare the convective vigour of our models to the Earth.

[insert table 1 about here]

Besides of table 1, results are presented graphically in figures 4 and 5. Temperature evolution plots (TEP) display the laterally averaged temperature profile versus time in a contour plot.

Accordingly, degassing evolution plots (DEP) are based on laterally averaged profiles of the concentration of pristine material. The scale of heterogeneity in the distribution of degassed material is determined by a spherical harmonic analysis. We applied the method used by Yang (1997) to the field of concentration minus the mean concentration at each radial level. The resulting spectral heterogeneity map (SHM) is a contour plot of the rms amplitude of the scalar field at different depths for spherical harmonic degrees 0 to 30. The colour scale of each plot is given as percentage of the maximum value occurring in that plot for all degrees and depths. A spherical harmonic analysis is only done for the last time step, corresponding to the modern Earth. The planform of the radial velocity component at 65 and 2825 km depths is given for three time steps. Only each group of three pictures shares a colour scheme. Cutaway views of the mantle show the degassing field at the same time steps as the velocity planform pictures. All cutaway views use the same colour scheme. Since some parameter variations have minor influence on the convective flow, pictures are only given for selected models.

[insert figures 4 and 5 about here]

4.3. Discussion

Mean surface velocities in all models are smaller than the observed value of 3.9 cm a^{-1} (Gordon and Jurdy, 1986) and the observed maximum velocities of more than 10 cm a^{-1} are not reached either. O'Connell et al. (1991) estimate that ~45 % of the Earth's surface velocity field is in toroidal components, but our models all display less than 5 %. Further shortcomings are discussed in Walzer et al. (2004b). However, currently there is no model of the Earth that satisfies all main constraints. The behaviour of the lithosphere at plate boundaries is determined by small-scale phenomena (fluids, melt, cracking and elasticity) that are not resolved in our global models. Besides a more realistic lateral variability of rheology, coupling between different scales is desirable in future models. Especially the outer boundary needs improvement but the deep mantle could still be adequately represented here. We do not attempt to relate the timescale of our models to the real Earth. Despite the rather low convective vigour (measured by surface velocity), we find degassing depths between 62 and 258 km, which are in the same order of magnitude as concluded by other studies: 60 – 115 km (Hirth and Kohlstedt, 1996), 65 km (Regenauer-Lieb and Kohl, 2003) and the depth of partial melting (< 200 km: Presnall et al., 2002).

4.3.1. Influence of geometry

In model A, no radial viscosity variation is assumed. This is certainly unrealistic for the Earth, but most clearly demonstrates an effect of 3-d spherical geometry. Thermal convection in general is organised in cell-like structures, which may vary in their shape, symmetry, size and time dependence. Let's consider a single roll of constant angular velocity in an incompressible, isoviscous cube. There is a line of pure rotation through the centre of the roll, which lies at mid-depth in the cube. Conservation of mass requires that flux through a vertical plane below this stagnation line equals the flux through a plane above the line. Now let's shrink the bottom of the cube, making it a frustum of an upside down pyramid. The stagnation line will move upwards until the flux through the vertical plane above the line is the same as below. This is analogous to what happens in 3-d spherical geometry. The assumption of constant angular velocity is certainly not realistic and asymmetries in the velocity distribution of a cell will overlay the illustrated geometric effect. For example, the planform area of upwellings may be smaller or larger than that of downwellings, depending on the model and even depth. A detailed investigation of the implications and relative importance of these aspects is beyond the scope of this paper. In A

degassed material from the top sinks right to the bottom of the mantle. There is only little hindrance at the depth of nonzero c_t, because viscosity is increased locally in cold downwellings. In lateral average degassed material fills the mantle from the bottom. The upper half of the mantle keeps its pristine signature for the longest time. This is due to the combined effects of cell geometry, flux asymmetry and lateral averaging. The latter just means that there is less volume in the LM for the same amount of degassed material than in the UM, giving LM a more degassed signature on average.

4.3.2. Influence of rheology

Model B is identical to A except for the viscosity profile. Downwellings are hindered and partially deflected, when they hit the high viscosity zone (HVZ) in the mid LM. This is evident in the first cutaway view and the high concentration of degassed material in about 1500 km depth during the first billion years of evolution. Furthermore the long-term preservation of pristine material in the upper half of the mantle is more pronounced than in A, with the lowest concentration of degassed material even closer to the surface. Velocities are lower in the HVZ of the lower mantle and consequently stagnation points of whole-mantle cells move further upwards. This effect is an additional reason for the more degassed signature of the LM. It has been observed in axisymmetrical models (van Keken et al., 2001) and even in Cartesian geometry (Ferrachat and Ricard, 2001). A distinct concentration gradient at 1500 km depth is maintained after ~1.5 Ga. This suggests that there is some degree of decoupling. Cold material sinks efficiently into the HVZ and produces long-wavelength heterogeneity there due to sluggish stirring. On the other hand, ambient upwelling from the HVZ delivers an average, less degassed signature upwards. The planform of radial velocity shows that the area of up- and downwellings is about equal in the HVZ but in the UM downwellings are narrow.

This is also true for the planform of model F, where the lower LVZ has been omitted. However, $l \sim 7$ heterogeneity is dominant throughout the mantle. This is a notable difference to B, where heterogeneity is pronounced in the HVZ. During its way down degassed material is stirred more efficiently, allowing only smooth concentration gradients in the lateral average. We conclude that the second asthenosphere is crucial for the decoupling of the stirring behaviour in the mid mantle. Support for that conclusion comes from model G, which features the lower LVZ but a stiffer lithosphere plus yielding. That variation hinders convection as indicated by lower surface velocities. In the first billion years degassed material is dispersed in the upper half of the mantle, similar to F. When the stable initial temperature profile is overcome, large cells fill the mantle from the bottom with degassed material. At the end, heterogeneity is pronounced in the HVZ. Hence the resulting layering of stirring behaviour is not an artefact of the early mode of dispersion in the model.

Compared to G, the viscosity profile for H and I has a slightly thicker and stiffer lithosphere. This minor change triggers a rather different evolution. During the first billion years convection is hindered by the phase boundary and viscosity increase in 660 km depth, combined with the effects of the stable initial temperature profile and the stiffer lithosphere. Small-scale cells develop which efficiently disperse degassed material in the upper mantle. After about 1.5 Ga the boundary between the vigorous convecting zone and pristine mantle moves down through the second LVZ until it reaches the HVZ of the lower mantle. While hindered there, degassed material is effectively stirred in the upper half of the mantle. However, the band of less degassed material in the DEP at 500 km depth extends to at least 3 Ga. A less visible band develops at 1000 km depth. This indicates, that there are still some cells confined to the UM. Other cells are operating between the two asthenospheres, with their stagnation points in the stiffer transition zone. Between 3 and 4 Ga the lower half of the mantle starts to convect and the system switches

to long wavelength convection. Regions with persisting small-scale convection are dragged into the mantle by this catastrophic overturn. No stability analysis (e.g. like Turcotte and Schubert, 2001, p. 270) has been carried out, but obviously that behaviour may be explained as follows. Small-scale convection efficiently cools the upper half of the mantle, but it is not able to penetrate into the HVZ, where longer wavelength perturbations are unstable. Further cooling of the upper half and heating of the lower half increases the Rayleigh number of the whole system, finally leading to the rise of the lower layer. The long wavelength of that rising layer is thereby overprinted on the entire mantle. Walzer and Hendel (1999) found a similar behaviour in a 2-d convection-differentiation model without stable initial stratification. The different yield stresses in H and I have only a gradual influence.
Profile *η6* in the otherwise identical model K initially leads to medium scale cells in the upper half of the mantle. There is no significant layering at the high viscosity transition zone or the phase boundary at 660 km depth, but instead at the lower HVZ. Large-scale overturn takes over before the upper half of the mantle is well stirred. This difference from models H and I is possibly due to the longer wavelength of the initial convection in the upper half of the mantle.
Profiles *η5* and *η6* are compared again in models J and R, but with an unstable initial temperature profile. There is insignificant or no layering of convection now. In both models, degassed material sinks from the top to the CMB in large-scale cells from the beginning. As in B, stagnation points occur in the upper 1000 km of the mantle (pronounced in J) and heterogeneity is expressed mostly in the lower HVZ (pronounced in R).

4.3.3. Influence of initial conditions

The comparisons of H versus J and K versus R indicate, that stable initial layering is necessary to confine early convection to the upper layers of the mantle. This conclusion is supported by L versus M, which differ only in their initial temperature profiles. Layering on top of the lower HVZ is much weaker in M, which has an unstable initial profile. As demonstrated by A and B, stable initial layering is not sufficient to trigger layered convection. Walzer et al. (2004b) find the small-scale convective regime also in 2-d models with unstable initial temperature profiles, but with larger viscosity differences in the UM.

4.3.4. Minor influences

According to (10) a higher melting temperature acts like an increased lateral temperature dependence of viscosity (c_t) at a given depth, and the volcanism module (*vol**) simply removes unrealistic peak temperatures. It follows from N versus O, that this difference affects degassing and global thermal history only slightly.
The thermal boundary at the CMB could affect the temperature profile and therefore has the potential to alter the whole evolution. However, comparison of models with core evolution versus constant heat flux (M versus N and P versus O) shows no significant difference in their degassing histories. The same is also true for D versus E, which feature different concentrations of ^{40}K in the core. All models with core evolution develop higher CMB heat fluxes than assumed for the other models. This leads to steeper thermal boundaries at the bottom. A wider parameter space ought to be explored, especially for the influence of the CMB heat flow in models with stable initial layering.

5. Conclusions

Despite the deficiencies of our models the following conclusions are considered to be reasonably robust for Earth-like parameters: (1) During large-scale convection in 3-d spherical geometry with a highly viscous LM, the upper 1000 km of the mantle are least affected by material that was

subject to differentiation near the surface. (2) Realistic radial viscosity variations -with two low viscosity zones in the upper half of the mantle and a highly viscous LM- result in a layering of the stirring behaviour. (3) Small-scale convection confined to the upper parts of the mantle is possible under certain conditions. (4) The convective regime may change from small-scale to large-scale convection.
The timescale in our models is unlikely to correspond to the real Earth, because surface velocities are smaller than observed, the viscosity profile does not evolve and we only speculate about the initial conditions.

5.1. Relevance for the Earth

We promote the following cartoon (figure 6) to be considered in the list of possible scenarios for the convection-differentiation history of the Earth.

[insert figure 6 about here]

There may have been layered convection in the Archean mantle. CC is extracted near the surface and the residuum is well stirred by small-scale cells in the uppermost convecting layer, as in models H and I. A layer of homogeneous depleted material may grow on top of pristine mantle, as found in a convection-differentiation model of Walzer and Hendel (1999). The depleted layer is not necessarily confined to the UM and the boundary between both regions is irregular.
At some stage the system must have switched to the style of convection, which is favoured for the Earth today. There are downwellings plunging from the surface into the lower mantle or even to the CMB. Because of 3-d spherical geometry and high viscosity in the lower mantle the stagnation points of the cell-like convective structures lie at rather shallow depths. Additionally, broad up- and small downwellings would fill the mantle from the bottom with degassed material and rise old material that has been there before. Laterally averaged, material just below the depth of partial melting can preserve its original signature for the longest time. The original signature may be the depleted signature that is left from the episode of small-scale convection. Stirring is less effective in the HVZ of the lower mantle and heterogeneities can persist there longer than in other parts of the mantle. Primordial material could have survived there, or, if stabilized by higher density (Tolstikhin and Hofmann, 2004), in D". Inefficient stirring in the HVZ also provides a mechanism to store recycled lithosphere for some time to develop high $^{3}He/^{4}He$ signatures as suggested by Ferrachat and Ricard (2001). Toroidal components and plate velocities at the surface are larger in the real Earth than in our models. Therefore stirring of the MORB source is probably underestimated here and the heterogeneity contrast to the HVZ in the LM may be even larger in the real Earth. A filter operating in the transition zone (Bercovici and Karato, 2003) is not essential in this proposal, but may help to maintain a homogeneous depleted MORB reservoir.
Reasons for a change in the convective regime are speculative. The overcoming of initially stable layering – thermally or compositionally – might be a possibility. An impermeable boundary in the mid mantle is unlikely today, but compositional layering may have contributed to convective isolation of lower parts of the mantle in the early Earth. Layering is more sustainable with higher convective vigour (Davaille, 1999, Oldham, 2004). Therefore it is also likely that the phase boundaries (Tackley, 1996) and steep viscosity gradients (Walzer and Hendel, 1999) had a stronger layering effect in a more vigorous regime. Almost certainly the viscosity was generally lower in the Archean. Radiogenic heating has been steadily decreasing. Both effects support higher convective vigour in the early Earth and likely had the potential to change the convective style of the mantle. In our models the viscosity profile is fixed for each run, gradients are

smoothed for numerical reasons and composition is uniform. Therfore layered convection in the Earth could have lasted longer than in the models – opposite to the effect of too small convective vigour on the model timescale. In the light of these competing shortcomings we can not determine the duration of the layered period or the percentage of mantle processed from our models.
Additional feedback could come from spatially inhomogeneous radiogenic heating, with the pristine lower layer being heated more than the depleted layer. The proposed change in the style of subduction (Xie and Tackley, 2003) could be contributing to or resulting from a change of the convective mode.
Two extreme scenarios are conceivable for the transition from small- to large-scale convection. One is the catastrophic overturn, captured in its initial stage by models H and I. The overturn is driven by the globally unstable layering and could result in a large-scale inversion of geochemical signatures, with pristine on top of degassed material. This is the opposite of what is being concluded from OIB and MORB signatures (Ballentine et al., 2002). Ballentine et al. (2002) also argue that this kind of overturn results in rising upper mantle temperatures but this is not observed in the laterally averaged temperature profiles of H and I. The other scenario is more like that occurring in model G. Large-scale cells appear early, but are accompanied by small-scale cells. The small cells die out, leaving behind a well-stirred, depleted upper part of the mantle. Then large-scale convection takes over without catastrophic overturn. At some stage the existing long wavelength cells just start to penetrate the lowermost mantle. Local instabilities rather than unstable global layering control this onset of deep subduction. The second scenario is favoured here, but both are only a small change in lithospheric rheology apart (see discussion G versus H) and hence aspects of both may have been operating in the Earth. Neither mechanism has been investigated in detail as yet. Models G, H, and I show only certain aspects of each.

5.2. Other hints for a change of convective mode

A consequence of the scenario outlined above is that the upper parts of the mantle are heterogeneous in the early stages of small-scale convection and more homogeneous before the onset of large-scale convection. Large-scale convection increases heterogeneity again, leading to the modern geochemical scatter in mantle-derived rocks. Rare earth signatures in picrites and komatiites from the Late Archean are indeed more homogeneous than in samples from the Early Archean, Proterozoic and Phanerozoic respectively (Campbell, 1998).
Breuer and Spohn (1995) propose a flush instability to explain geological and climate changes at the Archean-Proterozoic transition. There are several indications for rapid growth of CC, continents and ocean water mass during that time (see section 2.1. and discussion in Breuer and Spohn, 1995). CC growth is attributed to increasing UM temperatures, convective vigour and the lower mantle reservoir becoming available for CC extraction. Increased degassing of the mantle could lead to increased ocean water mass. This would be consistent with the catastrophic overturn scenario. Archean island-arc magmas originated in relatively warm, basaltic crust at lower pressures than at present, which could be explained by a smaller plate scale (Taylor and McLennan, 1995). Based on supercontinent cycles and greenstone ages, Condie (1997) favours layered convection before 2.8 Ga bp, episodicity of catastrophic overturn and hindering of deep subduction until 1.3 Ga bp and large-scale convection afterwards. Allègre (2002) reviews geochemical constraints and concludes that they are consistent with layered convection earlier and large-scale convection today. Breuer and Spohn (1995), Condie (1997) and Allègre (2002) assume the phase boundary at 660 km depth leads to temporal layering. However, their general arguments are also valid for the types of layering discussed here.

5.3. Outlook

Future models aiming at the reconciliation of geophysical and geochemical constraints may consider the following points:
(1) Global stirring studies need to account for 3-d spherical geometry. (2) One or more changes of the convective mode during the evolution of the mantle are a possibility. (3) Rheology has a strong influence on the stirring properties of the mantle. Shortcomings of our models are static viscosity profiles and an oversimplified lithospheric rheology that yields unrealistic (toroidal) velocities at the surface. Viscosity profiles should evolve according to the mantle temperature and more realistic lateral viscosity variations need to be included. (4) Neither trace element nor major element compositional differences have been modelled here. A more direct comparison of models and observations would be possible by coupling the evolution of isotopic systems (like Xie and Tackley, 2003) or reservoirs (like Walzer and Hendel, 1999) to models of mantle convection. Inhomogeneous internal heating, different densities and viscosities could provide a feedback on thermal convection. (5) We need a rational vision of Precambrian scenarios. Was there stable compositional or thermal layering? What was the tectonic style of the early Earth and how did chemical differentiation work, especially the segregation of CC?
As a working assumption we propose a marble cake like structure for the modern mantle, with small-scale geochemical structure dominating in the MORB source and heterogeneities larger than the sampling volume of deep-rooted plumes occurring in the LM. This includes segregation and temporal or permanent storage of dense recycled material above the CMB. The more homogeneous structure of the shallow mantle could be a leftover from an episode of small-scale convection and differentiation near the surface, combined with the effects of 3-d spherical geometry and the viscosity profile. Primitive material is most likely to have survived in the poorly mixed HVZ in the mid LM. It may reach the UM only as small-scale veins that are homogenised during sampling. A pure recycling model (Coltice and Ricard, 2002) is also conceivable. The relative importance and time-dependence of additional mechanisms, like zoning by variable depth of subduction (Albarède and van der Hilst, 2002), a filter contributing to the homogeneity of DMM (Bercovici and Karato, 2003), differences during melt extraction and the statistical nature of sampling (Meibom and Anderson, 2003) and the possibility of a doming regime (Davaille, 1999) with dense piles in upwellings (Tackley, 2000) may be investigated in more sophisticated future models.

Acknowledgements

The calculations for this paper were done on the supercomputers of the John-von-Neumann Institute for Computing at Forschungszentrum Jülich (Germany). We thank Doris Breuer, Thomas Burghardt, Nicolas Coltice, Sylvaine Ferrachat, Wolfgang Jacoby, Gerhard Jentzsch and Lothar Viereck-Götte for helpful discussions. Thorough reviews of Dave Yuen and an anonymous referee are appreciated.

References

Albarède, F., 2001, Earth Planet. Sci. Lett., 189, 59.
Albarède, F., and van der Hilst, R., 2002, Phil. Trans. R. Soc. Lond. A, 360, 2569.
Allègre, C. J., and Turcotte, D. L., 1986, Nature, 323, 123.
Allègre, C. J., and Lewin, C., 1995, Earth Planet. Sci. Lett., 136(34), 62946.
Allègre, C. J., 1997, Earth Planet. Sci. Lett., 150, 1.
Allègre, C. J., 2002, Phil. Trans. R. Soc. Lond. A, 360, 2411.
Allègre, C. J., Hamelin, B., Provost, A., and Dupre, B., 1987, Earth Planet. Sci. Lett., 81, 319.
Allègre, C. J., Hofmann, A., and O'Nions, K., 1996, Geophys. Res. Lett., 23, 3555.

Anderson, O. L., 1998, Phys. Earth Planet. Int., 109, 179.
Arndt, N. T., 2004, *The Precambrian Earth: Tempos and events*, edited by Eriksson, P. G., Altermann, W., Nelson, D. R., Mueller, W. U., and Catuneanu, O., (Elsevier: Developments in Precambrian Geology, 12), chapter 2. 8., pp. 155-158.
Arrhenius, G., and Lepland, A., 2000, Chemical Geology, 169, 69.
Ballentine, C. J., van Keken, P. E., Porcelli, D., and Hauri, E. H., 2002, Phil. Trans. R. Soc. Lond. A, 360, 2611.
Baumgardner, J. R., 1983, PhD Thesis, Univ. of California, Los Angeles.
Baumgardner, J. R., and Frederickson, P. O., 1985, SIAM J. Numer. Anal., 22, 1107.
Becker, T. W., Kellogg, J. B., and O'Connell, R. J., 1999, Earth Planet. Sci. Lett., 171, 351.
Bercovici, D, and Karato, S.-I., 2003, Nature, 425, 39.
Boehler, R., 2000, Reviews of Geophysics, 38(2), 221.
Breuer, D., and Spohn, T., 1995, Nature, 378, 608.
Bunge, H.-P., and Baumgardner, J. R., 1995, Computers in Physics, 9(2), 207.
Bunge, H.-P., Richards, M. A., and Baumgardner, J. R., 1997, J. Geophys. Res., 102(B6), 11991.
Campbell, I. H., 1998, *The Earth's mantle: composition, structure and evolution*, edited by Jackson, I. (Cambridge University Press)
Christensen, U. R., 1989, Earth Planet. Sci. Lett., 95 (3-4), 382.
Christensen, U. R., and Hofmann, A. W., 1994, J. Geophys. Res., 99(B10), 19867.
Coltice, N., and Ricard, Y., 2002, Phil. Trans. R. Soc. Lond. A, 360, 2633.
Condie, K. C., 1997, *Plate tectonics and crustal evolution, 4th ed.*, (Butterworth-Heinemann)
Courtillot, V., Davaille, A., Besse, J., and Stock, J., 2003, Earth Planet. Sci. Lett., 205, 295.
Davaille, A., 1999, Nature, 402, 756.
DeVolder, B., Glimm, J., Grove, J., Kang, Y., Lee, Y., Pao, K., Sharp, D. H., and Ye, K., 2002, J. Fluids Engineering, 124, 29.
Dixon, J.E., Dixon, T.H., Bell, D.R., and R. Malservisi, 2004, Earth Planet. Sci. Lett., 222, 451.
Dziewonski, A. M., and Anderson, D. L., 1981, Phys. Earth Planet. Int., 25, 297.
Elkins-Tanton, L. T., Parmentier, E. M., and Hess, P. C., 2003, Meteoritics and Planetary Science, 38(12), 1753.
Ferrachat, S., and Ricard, Y., 1998, Earth Planet. Sci. Lett., 155(12), 75.
Ferrachat, S., and Ricard, Y., 2001, Geochem. Geophys. Geosys., 2000GC000092.
ForteA. M., MitrovicaJ. X., and Woodward, R. L., 1995, Geophys. Res. Lett., 22(9), 1013.
Glatzmaier, G. A., 1988, Geophys. Astrophys. Fluid Dyn., 43, 223.
Gordon, R. G., and Jurdy, D. M., 1986, J. Geophys. Res., 91, 12389.
Gottschaldt, K.-D., 2003, Dissertation, Friedrich-Schiller Universität, Jena.
Grand, S. P., van der Hilst, R. D., and Widiyantoro, S., 1997, Geol. Soc. Am. Today, 7(4), 1.
Gurnis, M., and G. F., Davies, 1986, J. Geophys. Res., 91 (B6), 6375.
Hanan, B. B., Blichert-Toft, J., Pyle, D. G., and Christie, D. M., 2004, Nature, 432, 91.
Hart, S., 1984, Nature, 309, 753.
Hart, S., and Zindler, A., 1989, *Mantle convection*, edited by Peltier, W. R. (Montreaux: Gordon and Breach science publishers S. A.).
Helffrich, G. R., and Wood, B. J., 2001, Nature, 412, 501.
Hirose, K., 2002, J. Geophys. Res., 107(B4), 10. 1029/2001JB000597.
Hirth, G., and Kohlstedt, D. L., 1996, Earth Planet. Sci. Lett., 144, 93.
Hofmann, A. W., 1997, Nature, 385, 219.
Karato, S.-I., and Li, P., 1992, Science, 255, 1238.
Karato, S.-I., Riedel, M. R., and Yuen, D. A., 2001, Phys. Earth Planet. Int., 127, 83.

Karato, S.-I., and Wu, P., 1993, Science, 260, 771.
Kellogg, J. B., Jacobsen, S. B., and O'Connell, R. J., 2002, Earth Planet. Sci. Lett., 204, 183.
Kellogg, L. H., Hager, B. H., and van der Hilst, R. D., 1999, Science, 283, 1881.
Kellogg, L. H., and C. A. Stewart, 1991, Phys. Fluids A, 3 (5), 1374.
Kellogg, L. H., and D. L. Turcotte, 1990, J. Geophys. Res., 95 (B1), 421.
Kleine, T., Mezger, K., Palme, H., and Münker, C., 2004, Earth Planet. Sci. Lett., 228, 109.
Kreemer, C., Holt, W. E., and Haines, A. J., 2002, http://sps.unavco.org/crustal_motion/dedt/.
Labrosse, S., 2003, Phys. Earth Planet. Int., submitted.
Labrosse, S., Poirier, J.-P., and Le Mouël, J.-L., 2001, Earth Planet. Sci. Lett., 190, 11.
Li, P., Karato, S.-I., and Wang, Z., 1996, Earth Planet. Int., 95, 19.
Manga, M., 1996, Geophys. Res. Lett., 23(4), 403.
Masters, G., Laske, G., Bolton, H., and Dziewonski, A., 2000, *Mineral physics and seismic tomography*, edited by Karato, S. I. (Washington, DC: AGU)
Meibom, A., and Anderson, D. L., 2003, Earth Planet. Sci. Lett., 217, 123.
Metcalfe, G., Bina, C. R. and J. M. Ottino, 1995, Geophys. Res. Lett., 22 (7), 743.
Montelli, R., Nolet, G., Dahlen, F. A., Masters, G., Engdahl, E. R., and Hung, S.-H., 2004, Science, 303, 338.
Moresi, L., and Solomatov, V., 1998, Geophys. J. Int., 133 (3), 669.
Nakagawa, T., and Tackley, P. J., 2004, Geophys. Res. Lett., submitted.
O'Connell, R. J., Gable, C. W., and Hager, B. H., 1991, *Glacial isostasy, sea level, and mantle rheology*, edited by Sabadini, K., Lambeck, K., Boschi, E. (Dordrecht: Kluwer Academic Publishers), pp. 535-551.
O'Nions, R. K., and Oxburgh, E. R., 1983, Nature, 306, 429.
Oganov, A. R., and Ono, S., 2004, Nature, 430, 445.
Oldham, D. N., 2004, PhD Thesis, Cardiff University.
Olson, P., Yuen, D. A. and D. Balsiger, 1984, J. Geophys. Res., 89 (B1), 425.
Ottino, J. M., 1989, *The kinematics of mixing: stretching, chaos, and transport*, Cambridge University Press.
Presnall, D. C., Gudfinnsson, G. H., and Walter, M. J., 2002, Geochim. Cosmochim. Acta, 66, 2073.
Ramage, A., and Walthan, A. J., 1992, *Proceedings of the Copper Mountain Conference on Iterative Methods*, (Copper Mountain, Colorado, volume 1).
Regenauer-Lieb, K., and Kohl, T., 2003, *Mineralogical Magazine: Special Issue in Honour of Kerry Rodgers*, edited by Hoskin, P., submitted.
Richards, M. A., Yang, W.-S., Baumgardner, J. R., and Bunge, H.-P., 2001, Geochem. Geophys. Geosys., 2000GC000115.
Ritsema, J., van Heijst, H. J., and Woodhouse, J., 1999, Science, 286, 1925.
Ritsema, J., van Heijst, H. J., and Woodhouse, J., 2000, Science Progress, 83, 243.
Rüpke, L., Phipps Morgan, J., Hort, M., Connolly, J., and Ranero, C., 2003, Geophys. Res. Abstr., 5.
Schmalzl, J., 1996, Geologica Ultraiectina, 140.
Schubert, G., Turcotte, D. L., and Olson, P., 2001, *Mantle convection in the Earth and planets* (Cambridge University Press).
Schweitzer, J., 2002, Geophys. J. Int., 151, 209.
Sidorin, I., Gurnis, M., and Helmberger, D. V., 1999, J. Geophys. Res., 104, 15005.
Silver, P. G., Carlson, R. W., and Olson, P. L., 1988, Annu. Rev. Earth Planet. Sci., 16, 477.
Smolarkiewicz, P. K., 1984, J. Comp. Physics, 54(2), 325.

Solomatov, V. S., 2000, *Origin of the Earth and Moon*, edited by Canup, R. M., Righter, K. (Tucson: University of Arizona press), pp. 323.
Stacey, F. D., 1992, *Physics of the Earth, 3rd ed*. (Brisbane: Brookfield Press).
Stegman, D. R., Richards, M. A., and Baumgardner, J. R., 2002, J. Geophys. Res., 107(B6), 10. 1029/2001JB000192
Steinbach, V., Yuen, D. A., and Zhao, W. L., 1993, Geophys. Res. Lett., 20, 1119.
Su, W. J., Woodward, R. L., and Dziewonski, A. M., 1994, J. Geophys. Res., 99(B4), 6945.
Tackley, P. J., 1996, Geophys. Res. Lett., 23(15), 1985.
Tackley, P., 1998, Earth Planet. Sci. Lett., 157, 9.
Tackley, P. J., 2000, Science, 288, 2002.
Tackley, P. J., and Xie, S., 2002, Phil. Trans. R. Soc. Lond. A, 360, 2593.
Taylor, R. S., and McLennan, S. M., 1995, Rev. Geophys., 33, 241.
Ten, A., Podladchikov, Yu. Yu., Yuen, D. A., Larsen, T. B. and A. V. Malevsky, 1998, Geophys. Res. Lett., 25 (16), 3205.
Ten, A., Yuen, D. A., Larsen, T. B. and A. V. Malevsky, 1996, Geophys. Res. Lett., 23, 2001.
Ten, A., Yuen, D. A., Podladchikov, Yu.Yu., Larsen, T. B., Pachepsky, E. and A. V. Malvesky, 1997, Earth Planet. Sci. Lett., 146, 401.
Tolstikhin, I., and Hofmann, A. W., 2004, Phys. Earth Planet. Int., in press.
Trampert, J., Deschampes, F., Resovsky, J., and Yuen, D., 2004, Science, 306, 853.
Trendall, A. F., 2002, *Precambrian sedimentary environments: A modern approach to depositional systems*, edited by Altermann, W., and Corcoran, P. L. (IAS spec. publ., 44, Blackwell), pp. 33-66.
Trompert, R., and Hansen, U., 1998, Nature, 395, 686.
Turcotte, D. L., and Schubert, G., 2002, *Geodynamics, 2nd ed.* (Cambridge University Press).
van der Hilst, R., 2004, Science, 306, 817.
van der Hilst, R., and Karason, H., 1999, Science, 283, 1885.
van der Hilst, R. D., Widiyantoro, S., and Engdahl, E. R., 1997, Nature, 396, 578.
van Keken, P. E., and Zhong, S., 1999, Earth Planet. Sci. Lett., 171, 533.
van Keken, P. E., Ballentine, C. J., and Porcelli, D., 2001, Earth Planet. Sci. Lett., 188, 421.
van Keken, P. E., and Ballentine, C. J., 1998, Earth Planet. Sci. Lett., 156(12), 1932.
van Keken, P. E., King, S. D., Schmeling, H., Christensen, U. R., Neumeister, D., and Doin, M. P., 1997, J. Geophys. Res., 102(B10), 22477.
van Thienen, P., 2003, Geologica Ultraiectina, 236.
Walzer, U., and Hendel, R., 1999, Phys. Earth Planet. Int., 112, 211.
Walzer, U., Hendel, R., and Baumgardner, J., 2003, *High Performance Computing in Science and Engineering ´03*, edited by Krause, E., and Jäger, W. (Springer), pp. 27-67.
Walzer, U., Hendel, R., and Baumgardner, J., 2004a, Tectonophysics, 384 (1-4), 55.
Walzer, U., Hendel, R., and Baumgardner, J., 2004b, *High Performance Computing in Science and Engineering '04*, edited by Krause, E., Jäger, W., and Resch, M. (Springer), submitted.
Weis, D., Bassias, Y., Gautier, I., and Mennessier, J.-P., 1989, Geochim. Cosmochim. Acta, 53, 2125.
Xie, S, and Tackley, P., 2003, Phys. Earth Planet. Int., submitted.
Yang, W.-S., 1997, PhD Thesis, University of Illinois, Urbana-Champaign.
Zaranek, S. E., and Parmentier, E. M., 2004, J. Geophys. Res. B, 10. 1029/2003JB002462.
Zerr, A., and Boehler, R., 1993, Science, 262, 553.
Zerr, A., and Boehler, R., 1994, Nature, 371, 506.
Zindler, A., and Hart, S., 1986, Annu. Rev. Earth Planet. Sci., 14, 493.

table 1: Summary of models contributing to this study. Rheology is determined by the viscosity profile denoted in column η, the numerical damping factor c_t and the yield stress σ_y. The melting temperature profile, volcanism model, boundary condition at the CMB and initial condition are given in columns T_m, *vol*, *CMB* and *IC* respectively. σ_y is in [10^8 Pa] and the concentration of ^{40}K in the core in column *CMB* in [ppm]. The results for rms (v_{rms}) and maximum (v_{max}) surface velocity are in [cm a^{-1}], the degassing depth d_d is in [km]. All are for the last time step.

figure 1: All models feature these radial profiles of (a) specific heat at constant volume, (b) Grüneisen parameter, (c) melting temperature T_m1, T_m2, T_m3 and (d) thermal expansivity.

figure 2: (a) Radial variation c_t1 of the numerical damping factor, if not constant, (b) viscosity profiles $\eta2$ and $\eta3$, (c) viscosity profiles $\eta4$ and $\eta5$, (d) viscosity profile $\eta6$. (a) and (b) are based on Walzer et al. (2003) and (d) on Walzer et al. (2004a).

figure 3: Radial profiles of (a) reference temperature T_r, (b) initial temperature (black) and maximum perturbation (red and green) for *IC1*, (c) *IC2* and (d) *IC3*. Dotted lines in figure (a) mark the phase boundaries, which are considered in the code.

figure 4: Results of selected models. Three cutaway views of the mantle are placed to the right of the letter that is denoting the model. They show the degassing field at the same time steps as the planform of the radial velocity component that is given below. The upper row always is for 65 km depth and the lower row is for 2825 km. Velocity is given in [cm a^{-1}] and each legend is valid for a whole row. Depicted time steps were chosen separately for each model. Degassing evolution plot (DEP) and temperature evolution plot are placed in the right column. Light colours in the DEP indicate undegassed material (white = 100 % pm). The legend is also valid for the cutaway views. Pictures of not displayed models (in brackets) are similar to: B ~ (C, D, E), H ~ (I), L ~ (K), M ~ (N, O, P, Q, R). The timescale of the models may not correspond to the real Earth.

figure 5: Spectral heterogeneity maps for the distribution of degassed material in the last time step of selected models. The grey scale depicts the percentage of the maximum value occurring in each individual plot for all degrees and depths.

figure 6: During an episode of layered convection CC is extracted near the surface, leaving behind a depleted, well stirred residue above deeper pristine material (a). Layered convection may have been supported by compositional stratification, a stable initial temperature profile, steep radial viscosity gradients or the dynamic effects of phase boundaries in combination with higher convective vigour in the early mantle. Later large-scale convection with deep subduction starts to work on this configuration (b). Further differentiation and segregation of CC takes place near the surface, but the shallow mantle is least affected by this and possibly retains a depleted, homogeneous signature. Additionally, stirring is least effective in the mid lower mantle, allowing primitive and recycled material to coexist for the longest time in the convecting mantle. High density components may segregate in D". The modern MORB source would be a leftover from the episode of small-scale convection plus variable contamination from the lower half of the mantle. Small-scale plumes sampling different regions of the heterogeneous lower mantle produce the observed scatter in OIB geochemistry (c).

model	η	c_t	σ_y	T_m	*vol*	*CMB*	*IC*	v_{rms}	v_{max}	d_d
A	$\eta 1$	$c_t 1$	-	$T_m 1$	-	*CMB1*	*IC1*	0.2	0.7	144
B	$\eta 2$	$c_t 1$	-	$T_m 1$	-	*CMB1*	*IC1*	1.5	2.7	64
C	$\eta 2$	$c_t 1$	-	$T_m 1$	-	*CMB1*	*IC3*	1.4	2.5	62
D	$\eta 2$	$c_t 1$	-	$T_m 1$	-	100	*IC2*	1.6	2.6	67
E	$\eta 2$	$c_t 1$	-	$T_m 1$	-	200	*IC2*	1.7	2.9	66
F	$\eta 3$	$c_t 1$	-	$T_m 1$	-	*CMB1*	*IC1*	1.7	2.6	69
G	$\eta 4$	1.0	1.8	$T_m 1$	*vol1*	*CMB1*	*IC1*	1.2	1.8	99
H	$\eta 5$	1.0	1.8	$T_m 1$	*vol1*	*CMB1*	*IC1*	0.5	1.4	163
I	$\eta 5$	1.0	1.4	$T_m 1$	*vol1*	*CMB1*	*IC1*	0.6	1.7	152
J	$\eta 5$	1.5	1.35	$T_m 3$	*vol2*	*CMB2*	*IC4*	0.7	1.4	148
K	$\eta 6$	1.0	1.4	$T_m 1$	*vol1*	*CMB1*	*IC1*	1.2	2.8	223
L	$\eta 6$	1.0	1.35	$T_m 1$	-	200	*IC2*	0.8	1.9	176
M	$\eta 6$	1.0	1.35	$T_m 1$	-	200	*IC3*	0.9	2.0	155
N	$\eta 6$	1.0	1.35	$T_m 1$	-	*CMB2*	*IC3*	0.6	2.2	150
O	$\eta 6$	1.0	1.35	$T_m 2$	*vol2*	*CMB2*	*IC3*	0.8	1.7	151
P	$\eta 6$	1.0	1.35	$T_m 2$	*vol2*	200	*IC3*	0.8	2.4	160
Q	$\eta 6$	1.75	1.35	$T_m 2$	*vol2*	200	*IC3*	0.7	2.1	144
R	$\eta 6$	1.5	1.35	$T_m 3$	*vol2*	*CMB2*	*IC4*	0.7	1.8	158

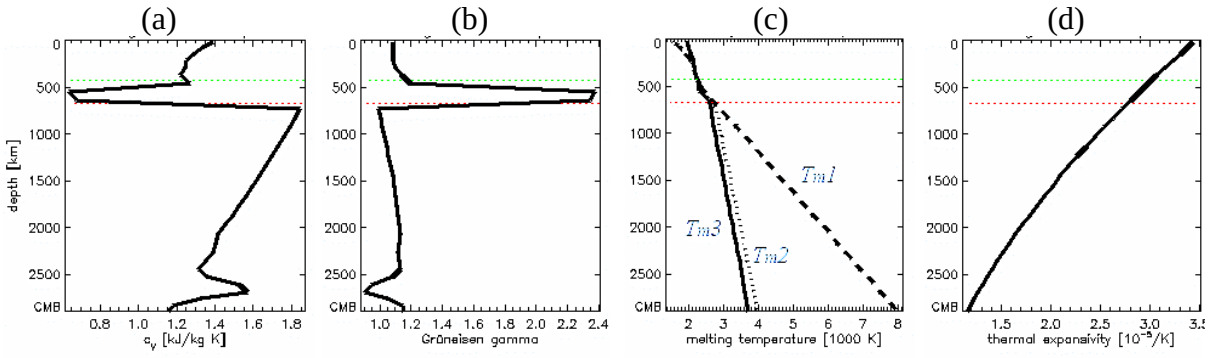
(a)
(b)
(c)
(d)
depth [km]
0
500
1000
1500
2000
2500
CMB
0.8 1.0 1.2 1.4 1.6 1.8
c_v [kJ/kg K]
1.0 1.2 1.4 1.6 1.8 2.0 2.2 2.4
Grüneisen gamma
2 3 4 5 6 7 8
melting temperature [1000 K]
Tm1
Tm2
Tm3
1.5 2.0 2.5 3.0
thermal expansivity [10^{-5}/K]

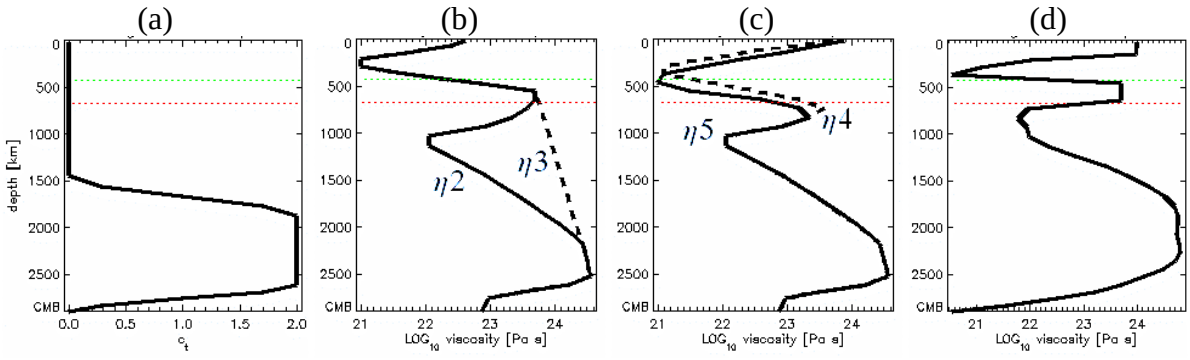
(a)
(b)
(c)
(d)
depth [km]
0
500
1000
1500
2000
2500
CMB
0.0
0.5
1.0
1.5
2.0
c_t
21
22
23
24
LOG_{10} viscosity [Pa s]
$\eta 2$
$\eta 3$
$\eta 4$
$\eta 5$

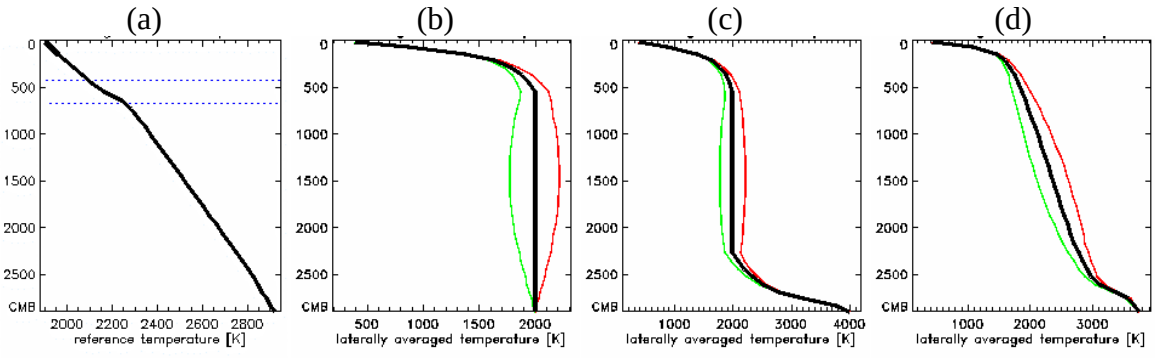
(a)
(b)
(c)
(d)
0
500
1000
1500
2000
2500
CMB
2000 2200 2400 2600 2800
reference temperature [K]
500 1000 1500 2000
laterally averaged temperature [K]
1000 2000 3000 4000
laterally averaged temperature [K]
1000 2000 3000
laterally averaged temperature [K]

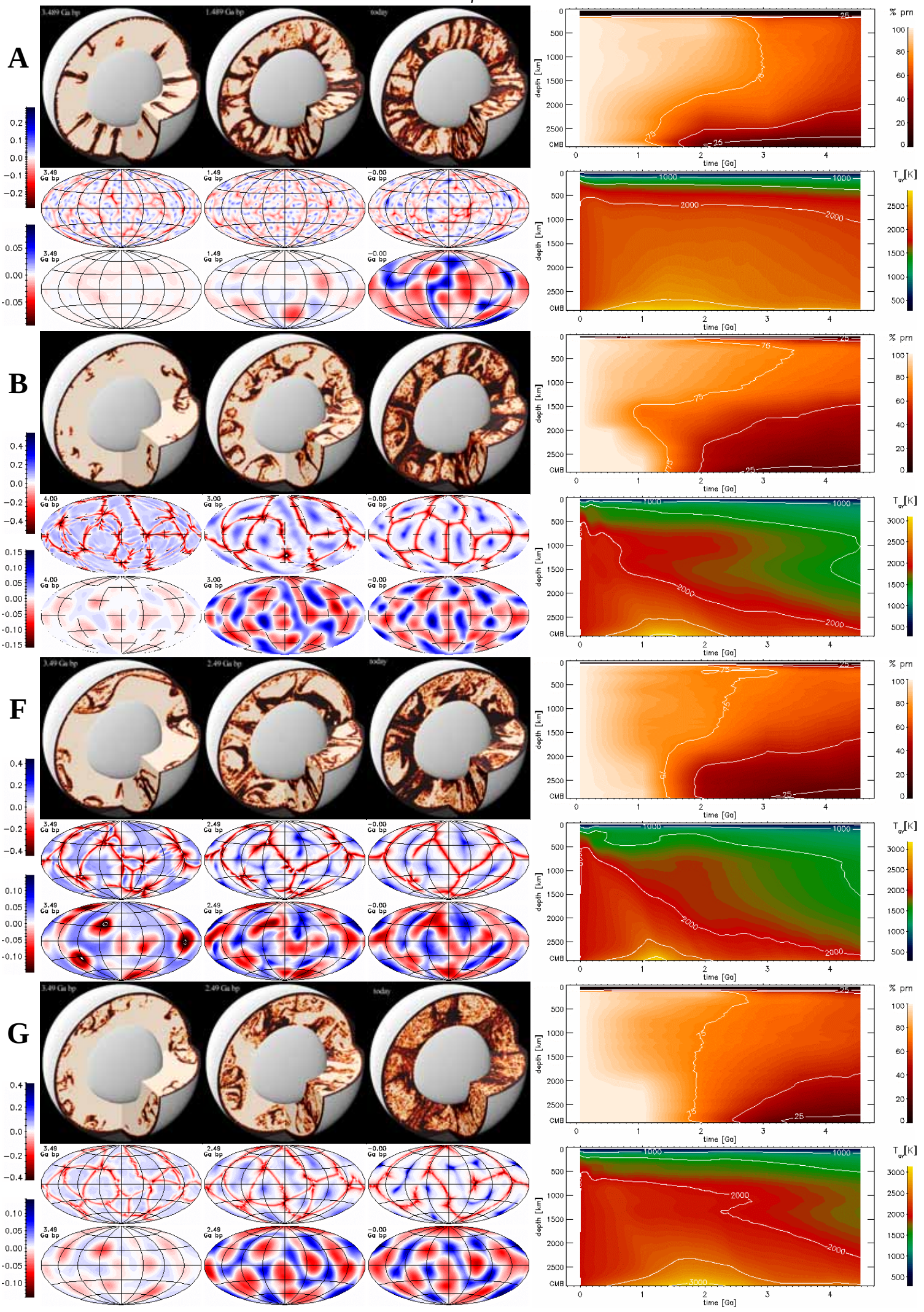

accepted for publication in Philosophical Magazine (www.PhilMag.net), 20 May 2005

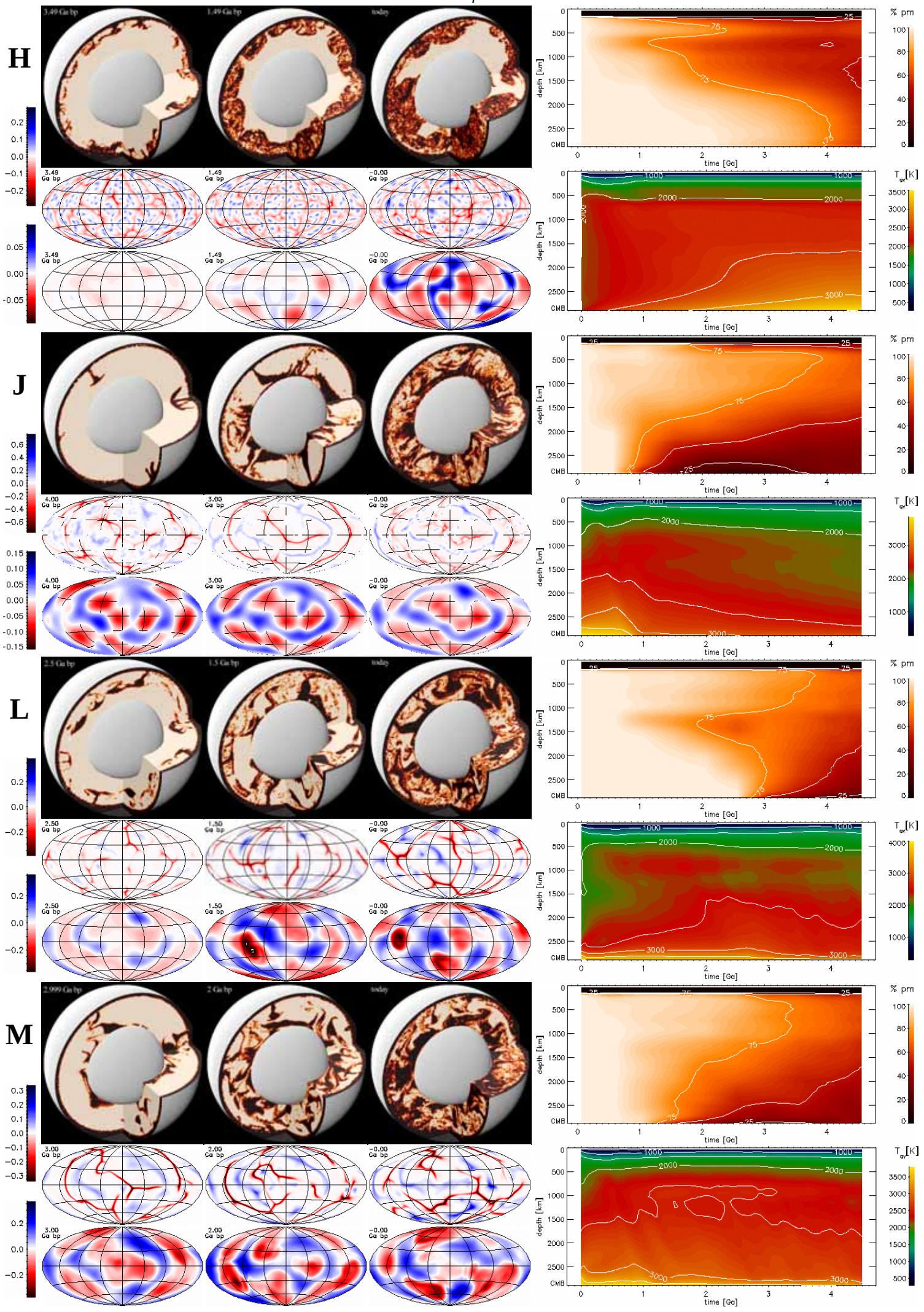
H
J
L
M
depth [km]
time [Ga]
% prn
T_av [K]
CMB

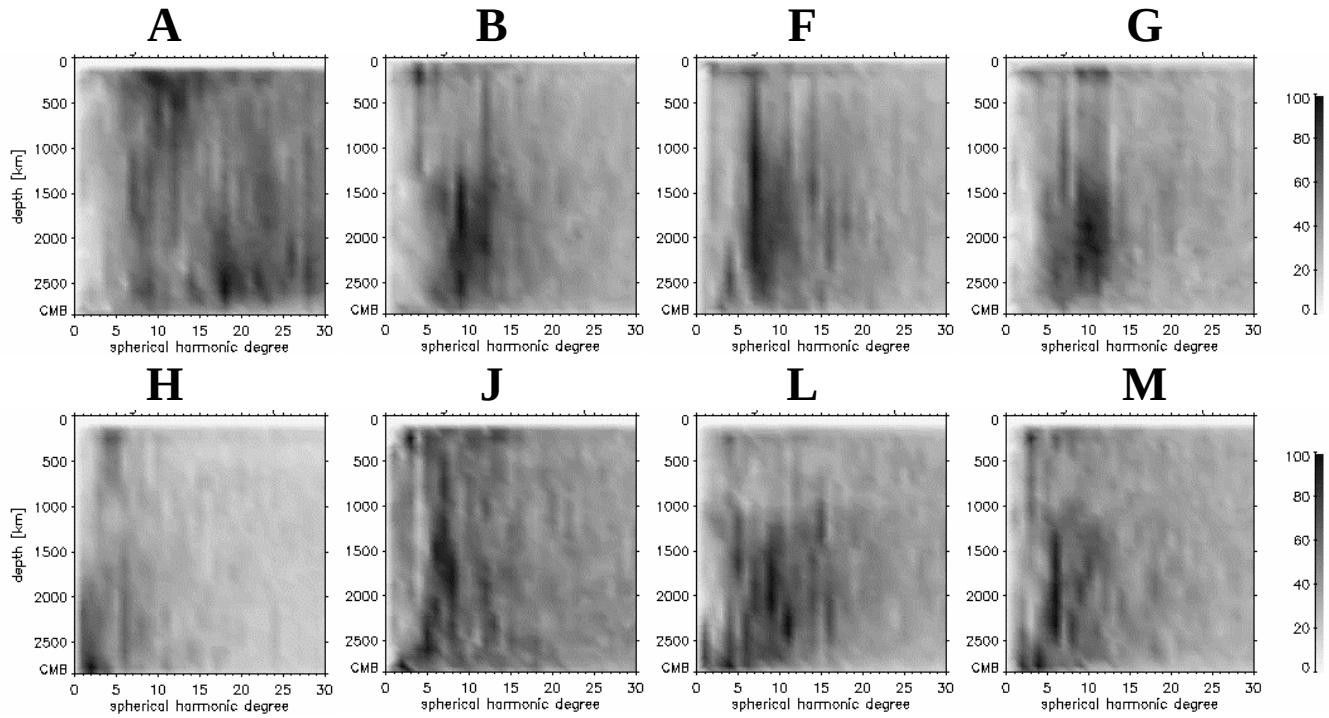
A
B
F
G
H
J
L
M
depth [km]
0
500
1000
1500
2000
2500
CMB
0 5 10 15 20 25 30
spherical harmonic degree
100
80
60
40
20
0

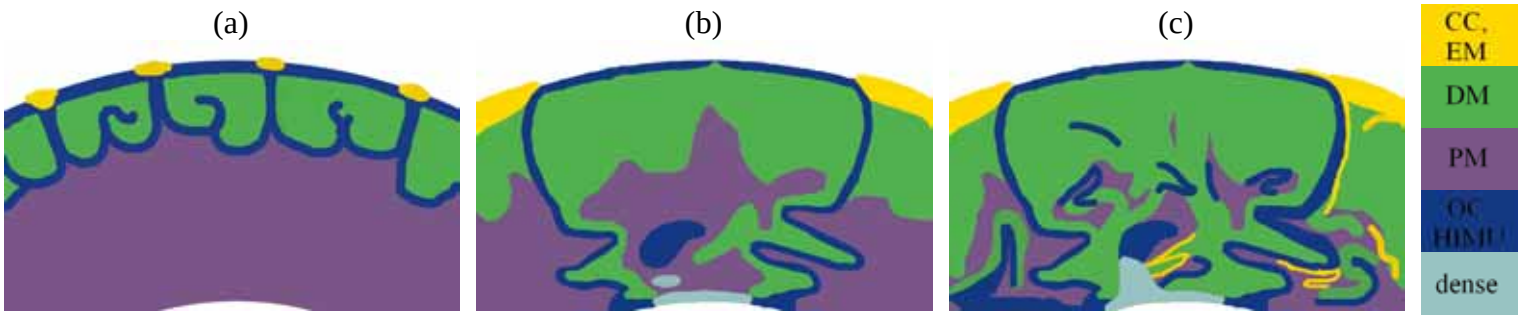
(a)
(b)
(c)
CC, EM
DM
PM
OC, HIM
dense